JHEP PROCEEDINGS

Corfu Summer Institute on Elementary Particle Physics, 1998

Two Lectures on QCD and Hadron Collider Physics

Michelangelo L. Mangano*

TH Division, CERN
1211 Geneva 23, Switzerland
michelangelo.mangano@cern.ch

ABSTRACT: I review in these lectures some simple applications of QCD to the physics of high-energy collisions, with explicit examples taken from recent Tevatron results.

KEYWORDS: QCD, partons, jets, hadronic collisions.

1. QCD and the proton structure at large Q^2

The understanding of the structure of the proton at short distances is one of the key ingredients to be able to predict cross-section for processes involving hadrons in the initial state. All processes in hadronic collisions, even those intrinsically of electroweak nature such as the production of W/Z bosons or photons, are in fact induced by the quarks and gluons contained inside the hadron. In this first lecture I will therefore introduce some important concepts, such as the notion of partonic densities of the proton, and of parton evolution. These are the essential tools used by theorists to predict production rates for hadronic reactions.

The idea that the parton language and the use of perturbative QCD can be used to describe the structure of the proton at short distances was developed in the late 60's and early 70's. While I will not provide you with a rigorous proof of the legitimacy of this approach, I will try to justify it qualitatively to make it sound at least plausible. More details can be found in good textbooks, such as those quoted in refs. [1]-[4]. I will then proceed to extract some results based on the application of perturbative QCD to lepton-hadron interactions.

1.1 The parton model

We all know that quarks are deeply bound inside the proton. It is important to realise, however, that the binding forces responsible for the quark confinement are due to the exchange of rather soft gluons. If a quark were to exchange a hard virtual gluon with another quark, in fact, the recoil would tend to break the proton apart. It is easy to verify that the exchange of gluons with virtuality larger than Q is then proportional to some large power of m_p/Q, m_p being the proton mass. Since the gluon coupling constant gets smaller at large Q, exchange of hard gluons is significantly suppressed [1]. As a result, the typical time scale for quarks inside the proton to interact among themselves is of the order of $1/m_p$, or longer. If we probe the proton with an off-shell photon, the interaction should take place during the limited lifetime of the virtual photon, given by the inverse of its virtuality as a result of the Heisenberg principle. Once the photon gets "inside" the proton and meets a quark, the struck quark has no time to negotiate a coherent response with the other quarks, because the time scale for it to "talk" to its pals is too long compared with the duration of the interaction with

*This work was supported in part by the EU Fourth Framework Programme "Training and Mobility of Researchers", Network "Quantum Chromodynamics and the Deep Structure of Elementary Particles", contract FMRX–CT98–0194 (DG 12 – MIHT).

[1] The fact that the coupling decreases at large Q plays a fundamental role in this argument. Were this not true, the parton picture could not be used!.

the photon itself. As a result, the struck quark has no option but to interact with the photon as if it were a free particle.

The one thing that the above picture does not tell us, obviously, is in which precise state the quark was once it got struck by the photon. This depends on the internal wave function of the proton, which perturbative QCD cannot easily predict. We can however say that the wave function of the proton, and therefore the state of the "free" quark, are determined by the dynamics of the soft-gluon exchanges inside the proton itself. Since the time scale of this dynamics is long relative to the time scale of the photon-quark interaction, we can safely argue that the photon sees to good approximation a static snapshot of the proton's inner guts. In other words, the state of the quark had been prepared long before the photon arrived. This also suggests that the state of the quark will not depend on the precise nature of the external probe, provided the time scale of the hard interaction is very short compared to the time it would take for the quark to readjust itself. As a result, if we could perform some measurement of the quark state using, say, a virtual-photon probe, we could then use this knowledge on the state of the quark to perform predictions for the interaction of the proton with any oter probe (e.g. a virtual W or even a gluon from an opposite beam of hadrons).

In order to make the measurement of the proton structure as simple as possible, it is therefore wise to use a probe as simple as possible. A virtual photon emitted from a beam of high-energy electrons provides such a probe. The relative process is called deeply inelastic scattering (DIS), and was historically the first phenomenon which led people to introduce the concept of partons.

Assuming the parton picture outlined above, we can describe the cross-section for the interaction of the virtual photon with the proton as follows:

$$\sigma_0 = \int_0^1 dx \sum_i e_i^2 \, f_i(x) \, \hat{\sigma}_0(\gamma^* q_i \to q_i', x) \quad (1.1)$$

where the 0 subscript anticipates that this description represents a leading order approximation. In the above equation, $f_i(x)$ represents the density of quarks of flavour i carrying a fraction x of the proton momentum. The hatted cross-section represents the interaction between the photon and a free (massless) quark:

$$\begin{aligned}
&\hat{\sigma}_0(\gamma^* q_i \to q_i') = \\
&\frac{1}{flux} \overline{\sum} |M_0(\gamma^* q \to q')|^2 \frac{d^3p'}{(2\pi)^3 2p_0'} \\
&\times (2\pi)^4 \delta^4(p' - q - p) \\
&= \frac{1}{flux} \overline{\sum} |M_0|^2 2\pi\delta(p'^2) \qquad (1.2)
\end{aligned}$$

Using $p' = xP + q$, where P is the proton momentum, we get

$$(p')^2 = 2xP \cdot q + q^2 \equiv 2xP \cdot q - Q^2 \qquad (1.3)$$

$$\hat{\sigma}_0(\gamma^* q \to q') = \frac{2\pi}{flux} \overline{\sum} |M_0|^2 \, \frac{1}{2P \cdot q} \, \delta(x - x_{bj}) \qquad (1.4)$$

where $x_{bj} = \frac{Q^2}{2P \cdot q}$ is the so-called Bjorken-x variable. Finally:

$$\begin{aligned}
\sigma_0 &= \frac{2\pi}{flux} \frac{\overline{\sum} |M_0|^2}{Q^2} \sum_i x_{bj} \, f_i(x_{bj}) \, e_i^2 \\
&\equiv \frac{2\pi}{flux} \frac{\overline{\sum} |M_0|^2}{Q^2} \, F_2(x_{bj}) \qquad (1.5)
\end{aligned}$$

The measurement of the inclusive ep cross-section as a function of Q^2 and $P \cdot q$ ($= m_p(E' - E)$ in the proton rest frame, with E' = energy of final-state lepton and E = energy of initial-state lepton) probes the quark momentum distribution inside the proton.

1.2 Parton evolution

Let us now study the QCD corrections to the LO parton-model description of DIS. This study will exhibit many important aspects of QCD (structure of collinear singularities, renormalization-group invariance) and will take us to an important element of the DIS phenomenology, namely scaling violations. We start from real-emission corrections to the Born level process:

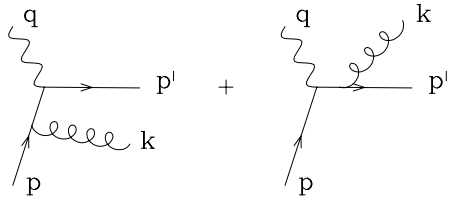

(1.6)

The first diagram is proportional to $1/(p-k)^2 = 1/2(pk)$, which diverges when k is emitted parallel to p:

$$p \cdot k = p^0 k^0 \ (1-\cos\theta) \stackrel{\cos\theta \to 1}{\longrightarrow} 0 \qquad (1.7)$$

The second diagram is also divergent, if k is emitted parallel to p'. This second divergence turns out to be harmless, since we are summing over all possible final states. Whether the final-state quark keeps all of its energy, or whether it decides to share it with a gluon emitted collinearly, an inclusive final-state measurement will not care. The collinear divergence can then be cancelled by a similar divergence appearing in the final-state quark self-energy corrections.

The first divergence is more serious, since from the point of view of the incoming photon (which only sees the quark, not the gluon) it *does* make a difference whether the momentum is all carried by the quark or is shared between the quark and the gluon. This means that no cancellation between collinear singularities in the real emission and virtual emission is possible. So let us go ahead, calculate explicitly the contribution of these diagrams, and learn how to deal with their singularities.

First of all note that while the second diagram is not singular in the region $k \cdot p \to 0$, its interference with the first one is. It is possible, however, to select a gauge for which the interference of the two diagrams is finite in this limit. You can show that the right choice is

$$\sum \epsilon_\mu \epsilon^*_\nu(k) = -g_{\mu\nu} + \frac{k^\mu p'^\nu + k^\nu p'^\mu}{k \cdot p'} \ . \qquad (1.8)$$

Notice that in this gauge not only $k \cdot \epsilon(k) = 0$, but also $p' \cdot \epsilon(k) = 0$. The key to getting to the end of a QCD calculation in a finite amount of time is choosing a proper gauge (which we just did) and the proper parametrization of the momenta involved. In our case, since we are interested in isolating the region where k becomes parallel with p, it is useful to set

$$k_\mu = (1-z)p_\mu + \beta p'_\mu + (k_\perp)_\mu \, , \qquad (1.9)$$

with $k_\perp \cdot p = k_\perp \cdot p' = 0$. β is obtained by imposing

$$k^2 = 0 = 2\beta(1-z)p \cdot p' + k_\perp^2 \qquad (1.10)$$

Defining $k_\perp^2 = -k_t^2$, we then get

$$\beta = \frac{k_t^2}{2(pp')\,(1-z)} \qquad (1.11)$$

$$k_\mu = (1-x)p_\mu + \frac{k_t^2}{2(1-x)p \cdot p'} \, p'_\mu + (k_\perp)_\mu \qquad (1.12)$$

$(k_\perp)_\mu$ is therefore the gluon momentum vector transverse to the incoming quark, in a frame where γ^* and q are aligned. k_t is the value of this transverse momentum. We also get

$$k \cdot p \ = \ \beta \, p \cdot p' = \frac{k_t^2}{2(1-z)} \qquad (1.13)$$

and

$$k \cdot p' \ = \ (1-z) p \cdot p' \qquad (1.14)$$

As a result $(p-k)^2 = -k_t^2/(1-z)$. The amplitude for the only diagram carrying the initial-state singularity is:

$$M_g \ = \ i g \lambda^a_{ij} \, \bar{u}(p') \Gamma \, \frac{\hat{p} - \hat{k}}{(p-k)^2} \, \hat{\epsilon}(k) u(p) \qquad (1.15)$$

(where we introduced the notation $\hat{a} \equiv \not{a} \equiv a_\mu \gamma^\mu$). We indicated by Γ the interaction vertex with the external current q. It is important to keep Γ arbitrary, because we would like to get results which do not depend on the details of the interaction with the external probe. It is important that the singular part of the QCD correction, and therefore its renormalization, be process independent. Only in this way we can hope to achieve a true universality of the parton densities! So we will keep Γ generic, and make sure that our algebra does not depend on its form, at least in the $p \cdot k \to 0$ limit. Squaring the most singular part of the amplitude, and summing over colours and spins, we get:

$$\sum_{\substack{\text{g polariz.} \\ \text{and colours}}} |M_g|^2 = g^2 \overbrace{\sum_a \text{tr}\,(\lambda^a \lambda^a)}^{N \times C_F} \times \frac{1}{t^2} \times$$
$$\sum_\epsilon \text{Tr}\,[\hat{p}' \, \Gamma (\hat{p} - \hat{k}) \, \hat{\epsilon} \ p \ \hat{\epsilon}^* \ (\hat{p} - \hat{k}) \ \Gamma^+] \qquad (1.16)$$

with $t = (p-k)^2 = -k_t^2/(1-z)$. Let us look first at

$$\sum_\epsilon \hat{\epsilon} \, \hat{p} \, \hat{\epsilon}^* \ = \ \sum \epsilon_\mu \, \epsilon^*_\nu \ \gamma^\mu \hat{p} \gamma^\nu \ = \ -\gamma^\mu \hat{p} \gamma^\mu +$$
$$\frac{1}{k \cdot p'} \, (\hat{p}' \hat{p} \hat{k} + \hat{k} \hat{p} \hat{p}')$$
$$= \ \frac{2}{1-z} \, (\hat{k} + \beta \hat{p}') \qquad (1.17)$$

(we used: $\hat{a}\hat{b}\hat{c}+\hat{c}\hat{b}\hat{a} = 2(a\cdot b)\,\hat{c} - 2(a\cdot c)\,\hat{b} + 2(b\cdot c)\,\hat{a}$ and some of the kinematical relations from the previous page). Then take

$$(\hat{p}-\hat{k})\,(\hat{k}+\beta\hat{p}')\,(\hat{p}-\hat{k}) = (\hat{p}-\hat{k})\,\hat{k}\,(\hat{p}-\hat{k}) + \beta(\hat{p}-\hat{k})\,\hat{p}'\,(\hat{p}-\hat{k}) \quad (1.18)$$

In the second term, proportional to β, we can approximate $\hat{k} = (1-z)\hat{p}$. This is because the other pieces $(\beta\hat{p}' + \hat{k}_\perp)$ multiplied by β would cancel entirely the $\frac{1}{t^2}$ singularity, and would only contribute a non-singular term, which we are currently neglecting. So Eq. (1.18) becomes

$$\begin{aligned}\hat{p}\hat{k}\hat{p} + \beta z^2 \hat{p}\hat{p}'\hat{p} &= 2(p\cdot k)\hat{p} + \beta z^2 2(p\cdot p')\hat{p} \\ &= 2(p\cdot k)\,(1+z^2)\hat{p} \end{aligned} \quad (1.19)$$

and

$$\begin{aligned}\sum |M_g|^2 &= 2g^2\,C_F\,\frac{(1-z)}{k_t^2}\,\left(\frac{1+z^2}{1-z}\right) \\ &\times\; N\,\mathrm{Tr}[\hat{p}'\Gamma\hat{p}\Gamma^+] \end{aligned} \quad (1.20)$$

The last factor with the trace corresponds to the Born amplitude squared. So the one-gluon emission process factorizes in the collinear limit into the Born process times a factor which is independent of the beam's nature! If we add the gluon phase-space:

$$\begin{aligned}[dk] &\equiv \frac{d^3k}{(2\pi)^3 2k^0} = \frac{dk_\parallel}{k^0}\,\frac{d\phi}{2\pi}\,\frac{1}{8\pi^2}\,\frac{dk_\perp^2}{2} \\ &= \frac{dz}{(1-z)}\,\frac{1}{16\pi^2}\,dk_\perp^2 \end{aligned} \quad (1.21)$$

we get:

$$\overline{\sum}|M_g|^2\,[dk] = \frac{dk_\perp^2}{k_\perp^2}\,dz\,\left(\frac{\alpha_s}{2\pi}\right)\,P_{qq}(z)\,\overline{\sum}|M_0|^2 \quad (1.22)$$

where

$$P_{qq}(z) = C_F\frac{1+z^2}{1-z} \quad (1.23)$$

is the so-called Altarelli-Parisi splitting function for the $q \to q$ transition (z is the momentum fraction of the original quark taken away by the quark after gluon emission). We are now ready to calculate the corrections to the parton-model cross-section:

$$\begin{aligned}\sigma_g &= \int dx\,f(x)\,\frac{1}{flux}\int dz\,\frac{dk_\perp^2}{k_\perp^2}\,\left(\frac{\alpha_s}{2\pi}\right)\,P_{qq}(z) \\ &\times\;\overline{\sum}|M_0|^2\,2\pi\delta(p'^2) \end{aligned} \quad (1.24)$$

Using $(p')^2 = (p-k+q)^2 \sim (zp+q)^2 = (xzP+q)^2$ and

$$\delta(p'^2) \;=\; \frac{1}{2P\cdot q}\,\frac{1}{z}\,\delta(x-\frac{x_{bj}}{z}) \;=\; \frac{x_{bj}}{z}\,\delta(x-\frac{x_{bj}}{z}) \quad (1.25)$$

we finally obtain:

$$\begin{aligned}\sigma_g \;=\; &\frac{2\pi}{flux}\,\left(\frac{\overline{\sum}|M_0|^2}{Q^2}\right)\,\sum_i e_i^2\,x_{bj}\,\frac{\alpha_s}{2\pi} \\ &\times\int\frac{dk_\perp^2}{k_\perp^2}\int\frac{dz}{z}\,P_{qq}(z)\,f_i\,\left(\frac{x_{bj}}{z}\right) \end{aligned} \quad (1.26)$$

We then find that the inclusion of the $\mathcal{O}(\alpha_s)$ correction is equivalent to a contribution to the parton density:

$$f_i(x) \to f_i(x) + \frac{\alpha_s}{2\pi}\int\frac{dk_\perp^2}{k_\perp^2}\int_x^1\frac{dz}{z}\,P_{qq}(z)\,f_i\left(\frac{x}{z}\right) \quad (1.27)$$

Notice the presence of the integral $\int dk_\perp^2/k_\perp^2$. The upper limit of integration is proportional to Q^2. The lower limit is 0. Had we included a quark mass, the propagator would have behaved like $1/(k_\perp^2+m^2)$. But the quark is bound inside the hadron, so we do not quite know what m should be. Let us then assume that we cut-off the integral at a $k_\perp$ value equal to some scale μ_0, and see what happens. The effective parton density becomes:

$$\begin{aligned}&f(x,Q^2) = f(x) + \\ &\log\left(\frac{Q^2}{\mu_0^2}\right)\,\frac{\alpha_s}{2\pi}\int_x^1\frac{dz}{z}\,P_{qq}(z)\,f\left(\frac{x}{z}\right) \end{aligned} \quad (1.28)$$

The dependence on the scale μ_0, which is a non-perturbative scale, can be removed by defining $f(x,Q^2)$ in terms of the parton density f *measured* at a large, perturbative scale μ^2:

$$\begin{aligned}&f(x,\mu^2) = f(x) + \\ &\log\left(\frac{\mu^2}{\mu_0^2}\right)\,\frac{\alpha_s}{2\pi}\int_x^1\frac{dz}{z}\,P_{qq}(z)\,f\left(\frac{x}{z}\right) \end{aligned} \quad (1.29)$$

We can then perform a subtraction, and write:

$$\begin{aligned}&f(x,Q^2) = f(x,\mu^2) + \\ &\log\left(\frac{Q^2}{\mu^2}\right)\,\frac{\alpha_s}{2\pi}\int_x^1\frac{dz}{z}\,P_{qq}(z)\,f\left(\frac{x}{z}\right) \end{aligned} \quad (1.30)$$

The scale μ plays here a similar role to the renormalization scale. Its choice is arbitrary, and $f(x,Q^2)$

should not depend on it. Requiring this independence, we get the following "renormalization-group invariance" condition:

$$\frac{df(x,Q^2)}{d\ln\mu^2} = \mu^2\frac{df(x,\mu^2)}{d\mu^2} - \frac{\alpha_s}{2\pi}\int_x^1\frac{dz}{z}P_{qq}(z)\,f\left(\frac{x}{z}\right)\equiv 0 \quad (1.31)$$

and then

$$\mu^2\frac{df(x,\mu^2)}{d\mu^2} = \frac{\alpha_s}{2\pi}\int_x^1\frac{dz}{z}P_{qq}(z)\,f\left(\frac{x}{z},\mu^2\right) \quad (1.32)$$

This equation is usually called the DGLAP (Dokshitzer-Gribov-Lipatov-Altarelli-Parisi) equation. As in the case of the resummation of leading logarithms in $R_{e^+e^-}$ induced by the RG invariance constraints, the DGLAP equation – which is the result of RG-invariance – resums a full tower of leading logarithms of Q^2.

Proof: Let us define $t=\log\frac{Q^2}{\mu^2}$. We can then expand $f(x,t)$ in powers of t:

$$f(x,t) = f(x,0)+t\frac{df}{dt}(x,0)+\frac{t^2}{2!}\frac{d^2f}{dt^2}(x,0)+\ldots \quad (1.33)$$

The first derivative is given by the DGLAP equation itself. Higher derivatives can be obtained by differentiating it:

$$\begin{aligned} f''(x,t) &= \frac{\alpha_s}{2\pi}\int\frac{dz}{z}P_{qq}(z)\frac{df}{dt}(\frac{x}{z},t)\\ &= \frac{\alpha_s}{2\pi}\int_x^1\frac{dz}{z}P_{qq}(z)\frac{\alpha_s}{2\pi}\\ &\times\int_{\frac{x}{z}}^1\frac{dz'}{z'}P_{qq}(z)f(\frac{x}{zz'},t)\\ &\vdots\\ f^{(h)}(x,t) &= \frac{\alpha_s}{2\pi}\int_x^1\ldots\ldots\frac{\alpha_s}{2\pi}\\ &\times\int_{x/zz'\ldots z^{(n-1)}}^1\frac{dz^{(n)}}{z^{(n)}}\\ &\times P_{qq}(z^{(n)})f(\frac{x}{zz'\ldots},t) \end{aligned} \quad (1.34)$$

The n-th term in this expansion, proportional to $(\alpha_s\,t)^n$, corresponds to the emission of n gluons (it is just the n-fold iteration of what we did studying the one-gluon emission case).

With similar calculations one can include the effect of the other $\mathcal{O}(\alpha_s)$ correction, originating from the splitting into a $q\bar{q}$ pair of a gluon contained in the proton. With the addition of this term, the evolution equation for the density of the ith quark flavour becomes:

$$\frac{df_q(x,t)}{dt} = \frac{\alpha_s}{2\pi}\int_x^1\frac{dz}{z}\left[P_{qq}(z)\,f_i(\frac{x}{z},t)+P_{qg}(z)f_g(\frac{x}{z},t)\right], \quad (1.35)$$

with

$$P_{qg}=\frac{1}{2}\left[z^2+(1-z)^2\right] \quad (1.36)$$

In the case of interactions with a coloured probe (say a gluon) we meet the following corrections, which affect the evolution of the gluon density $f_g(x)$:

$$\frac{df_g(x,t)}{dt} = \frac{\alpha_s}{2\pi}\int_x^1\frac{dz}{z}\left[P_{gq}(z)\sum_{i=q,\bar{q}}f_i\left(\frac{x}{z},t\right)+P_{gg}(z)f_g\left(\frac{x}{z},t\right)\right] \quad (1.37)$$

with

$$P_{gq}(z)=P_{qq}(1-z)=C_F\frac{1+(1-z)^2}{z} \quad (1.38)$$

and

$$P_{gg}(z)=2C_A\left[\frac{1-z}{z}+\frac{z}{1-z}+z(1-z)\right] \quad (1.39)$$

Defining the moments of an arbitrary function $g(x)$ as follows:

$$g_n=\int_0^1\frac{dx}{x}\,x^n\,g(x)$$

it is easy to prove that the evolution equations turn into ordinary linear differential equations:

$$\frac{df_i^{(n)}}{dt} = \frac{\alpha_s}{2\pi}[P_{qq}^{(n)}f_i^{(n)}+P_{qg}^{(n)}f_g^{(n)}] \quad (1.40)$$

$$\frac{df_g^{(n)}}{dt} = \frac{\alpha_s}{2\pi}[P_{gg}^{(n)}\,f_g+P_{gq}^{(n)}f_i^{(n)}] \quad (1.41)$$

1.3 Properties of the evolution equations

We now study some general properties of these equations. It is convenient to introduce the concepts of *valence* ($V(x,t)$) and *singlet* ($\Sigma(x,t)$)

densities:

$$V(x) = \sum_i f_i(x) - \sum_{\bar{\imath}} f_{\bar{\imath}}(x) \qquad (1.42)$$

$$\Sigma(x) = \sum_i f_i(x) + \sum_{\bar{\imath}} f_{\bar{\imath}}(x) \qquad (1.43)$$

where the index $\bar{\imath}$ refers to the antiquark flavours. The evolution equations then become:

$$\frac{dV^{(n)}}{dt} = \frac{\alpha_s}{2\pi} P_{qq}^{(n)} V^{(n)} \qquad (1.44)$$

$$\frac{d\Sigma^{(n)}}{dt} = \frac{\alpha_s}{2\pi} \left[P_{qq}^{(n)} \Sigma^{(n)} + 2n_f P_{qg}^{(n)} f_g^{(n)} \right] \qquad (1.45)$$

$$\frac{df_g^{(n)}}{dt} = \frac{\alpha_s}{2\pi} \left[P_{gq}^{(n)} \Sigma^{(n)} + P_{gg}^{(n)} f_g^{(n)} \right] \qquad (1.46)$$

Note that the equation for the valence density decouples from the evolution of the gluon and singlet densities, which are coupled among themselves. This is physically very reasonable, since in perturbation theory the contribution to the quark and the antiquark densities coming form the evolution of gluons (via their splitting into $q\bar{q}$ pairs) is the same, and will cancel out in the definition of the valence. The valence therefore only evolves because of gluon emission. On the contrary, gluons and $q\bar{q}$ pairs in the proton *sea* evolve into one another.

The first moment of $V(x)$, $V^{(1)} = \int_0^1 dx\, V(x)$, counts the number of valence quarks. We therefore expect it to be independent of Q^2:

$$\frac{dV^{(1)}}{dt} \equiv 0 = \frac{\alpha_s}{2\pi} P_{qq}^{(1)} V^{(1)} = 0 \qquad (1.47)$$

Since $V^{(1)}$ itself in different from 0, we obtain a constraint on the first moment of the splitting function: $P_{qq}^{(1)} = 0$. This constraint is satisfied by including the effect of the virtual corrections, which generate a contribution to $P_{qq}(z)$ proportional to $\delta(1-z)$. This correction is incorporated in $P_{qq}(z)$ via the redefinition:

$$P_{qq}(z) \to \left(\frac{1+z^2}{1-z} \right)_+ \equiv \frac{1+z^2}{1-z} - \delta(1-z) \int_0^1 dy \left(\frac{1+y^2}{1-y} \right) \qquad (1.48)$$

where the + sign turns $P_{qq}(z)$ into a distribution. In this way, $\int_0^1 dz\, P_{qq}(z) = 0$ and the valence sum-rule is obeyed at all Q^2.

Another sum rule which does not depend on Q^2 is the momentum sum rule, which imposes the constraint that all of the momentum of the proton is carried by its constituents (valence plus sea plus gluons):

$$\int_0^1 dx\, x \left[\sum_{i,\bar{\imath}} f_i(x) + f_g(x) \right] \equiv \Sigma^{(2)} + f_g^{(2)} = 1 \qquad (1.49)$$

Once more this relation should hold for all Q^2 values, and you can prove by using the evolution equations that this implies:

$$P_{qq}^{(2)} + P_{gq}^{(2)} = 0 \qquad (1.50)$$

$$P_{gg}^{(2)} + 2n_f P_{qg}^{(2)} = 0 \qquad (1.51)$$

You can check using the definition of second moment, and the explicit expressions of the P_{qq} and P_{gq} splitting functions, that the first condition is automatically satisfied. The second condition is satisfied by including the virtual effects in the gluon propagator, which contribute a term proportional to $\delta(1-z)$. It is a simple exercise to verify that the final form of the $P_{gg}(z)$ splitting function, satisfying eq. (1.51), is:

$$P_{gg} \to 2C_A \left\{ \frac{x}{(1-x)_+} + \frac{1-x}{x} + x(1-x) \right\} + \delta(1-x) \left[\frac{11C_A - 2n_f}{6} \right] \qquad (1.52)$$

1.4 Solution of the evolution equations

The evolution equations formulated in the previous section can be solved analytically in moment space. The boundary conditions are given by the moments of the parton densities at a given scale μ, where in principle they can be obtained from a direct measurement. The solution at different values of the scale Q can then be obtained by inverting numerically the expression for the moments back to x space. The resulting evolved densities can then be used to calculate cross sections for an arbitrary process involving hadrons, at an arbitrary scale Q. We shall limit ourselves here to studying some properties of the analytic solutions, and will present and comment some plots obtained from numerical studies available in the literature.

As an exercise, you can show that the solution of the evolution equation for the valence density is the following:

$$V^{(n)}(Q^2) = V^{(n)}(\mu^2)\left[\frac{\log Q^2/\Lambda^2}{\log \mu^2/\Lambda^2}\right]^{P^{(n)}_{qq}/2\pi b_0} = V^{(n)}(\mu^2)\left[\frac{\alpha_s(\mu^2)}{\alpha_s(Q^2)}\right]^{P^{(n)}_{qq}/2\pi b_0} \quad (1.53)$$

where the running of $\alpha_s(\mu^2)$ has to be taken into account to get the right result. Since all moments $P^{(n)}$ are negative, the evolution to larger values of Q makes the valence distribution softer and softer. This is physically reasonable, since the only thing that the valence quarks can do is to loose energy because of gluon emission.

The solutions for the gluon and singlet distributions f_g and Σ can be obtained by diagonalizing the 2×2 system in eqs. (1.45) and (1.46). We study the case of the second moments, which correspond to the momentum fractions carried by quarks and gluons separately. In the asymptotic limit $\Sigma^{(2)}$ goes to a constant, and $\frac{d\Sigma^{(2)}}{dt} = 0$. Then, using the momentum sum rule:

$$P^{(2)}_{qq}\,\Sigma^{(2)} + 2n_f\,P^{(2)}_{qg} f^{(2)}_g = 0 \quad (1.54)$$

$$\Sigma^{(2)} + f^{(2)}_g = 1 \quad (1.55)$$

The solution of this system is:

$$\Sigma^{(2)} = \frac{1}{1+\frac{4C_F}{n_f}} \quad (1.56)$$

$$f^{(2)}_g = \frac{4C_F}{4C_F + n_f} \quad (1.57)$$

As a result, the fraction of momentum carried by gluons is asymptotically approximately 50% of the total proton momentum. It is interesting to note that, experimentally, this asymptotic value is actually reached already at rather low values of Q^2. It was indeed observed already since the early days of the DIS experiments that only approximately 50% of the proton momentum was carried by charged constituents. This was one of the early evidences for the existence of gluons.

As I mentioned earlier, a complete solution for the evolved parton densities in x space can only be obtained from a numerical analysis. This work has been done in the past by several groups (see e.g. the discussions in ref. [4]), and is continuously being updated by including the most up-to-date experimental results used for the determination of the input densities at a fixed scale. Figure 1 (left side) shows the up-quark valence momentum density at different scales Q. Note the anticipated softening at large scales, and the clear $\log Q^2$ evolution. The most likely momentum fraction carried by a valence up quark in the proton goes from $x \sim 20\%$ at $Q = 3$ GeV, to $x \lesssim 10\%$ at $Q = 1000$ GeV. Notice finally that the density vanishes at small x.

The right plot in Figure 1 shows instead the gluon momentum density at different scales Q. This time the density grows at small-x, with an approximate $g(x) \sim 1/x^{1+\delta}$ behaviour, and $\delta > 0$ slowly increasing at large Q^2. This low-x growth is due to the $1/x$ emission probability for the radiation of gluons, and is represented by the $1/x$ factors in the $P_{gq}(x)$ and $P_{gg}(x)$ splitting functions.

Figure 2 (left) shows the up-quark *sea* momentum density at different scales Q. Shape and evolution match those of the gluon density, a consequence of the fact that sea quarks come from the splitting of gluons. Since the gluon-splitting probability is proportional to α_s, the approximate ratio $sea/gluon \sim 0.1$ which can be obtained by comparing the various plots is perfectly justified.

Finally, the momentum densities for gluons, up-sea, charm and up-valence distributions are shown in the right plot of fig.2 for $Q = 1000$ GeV. Note here that u_{sea} and charm are approximately the same at very large Q and small x, The proton momentum is mostly carried by valence quarks and by gluons. The contribution of sea quarks is negligible.

2. QCD in hadronic collisions

In hadronic collisions, all phenomena are QCD-related. The dynamics is more complex than in e^+e^- or DIS, since both beam and target have a non-trivial partonic structure. As a result, calculations (and experimental analyses) are more

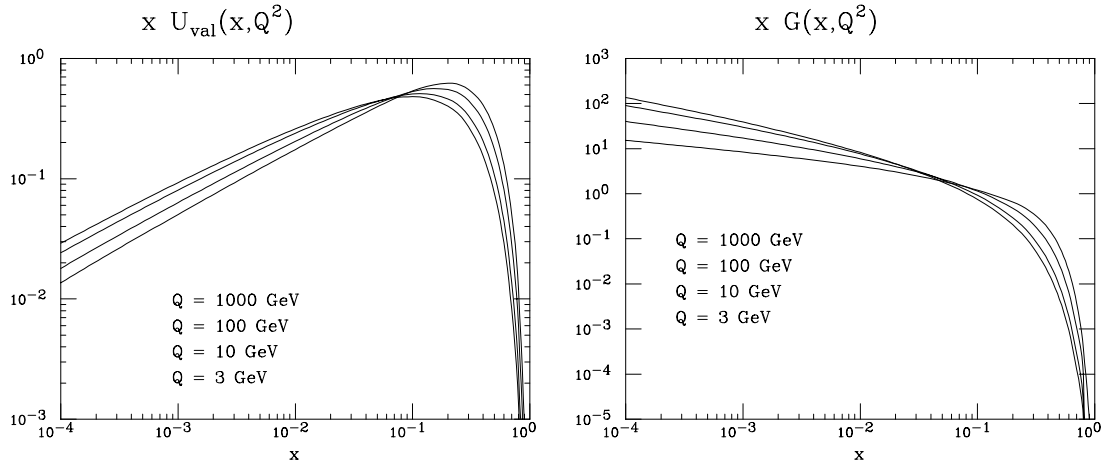

Figure 1: Left:Valence up-quark momentum-density distribution, for different scales Q. Right: gluon momentum-density distribution.

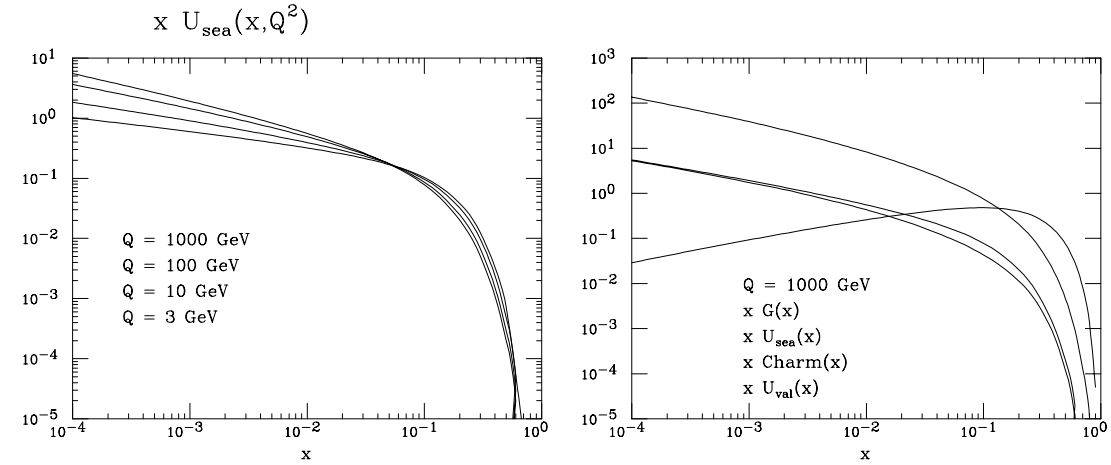

Figure 2: Left: Sea up-quark momentum-density distribution, for different scales Q. Right: Momentum-density distribution for several parton species, at $Q = 1000$ GeV.

complicated. QCD phenomenology is however much richer, and the higher energies available in hadronic collisions allow to probe the structure of the proton and of its constituents at the smallest scales attainable in a laboratory.

Contrary to the case of e^+e^- and lepton-hadron collisions, where calculations are routinely available up to next-to-next-to-leading order accuracy, theoretical calculations for hadronic collisions are available at best with next-to-leading-order (NLO) accuracy. The only exception is the case of Drell-Yan production, where NNLO results are known for the total cross sections. So we generally have relatively small precision in the theoretical predictions, and theoretical uncertainties which are large when compared to LEP or HERA.

However, $p\bar{p}$ collider physics is primarily *discovery* physics, rather than precision physics (there are exceptions, such as the measurements of the W mass and of the properties of b-hadrons. But these are not QCD-related measurements). As such, knowledge of QCD is essential both for the estimate of the expected signals, and for the evaluation of the backgrounds. Tests of QCD in $p\bar{p}$ collisions confirm our understanding of perturbation theory, or, when they fail, point to areas where our approximations need to be improved.

(see, e.g., the theory advances prompted by the measurements of ψ production at CDF!).

Finally, a reliable theoretical control over the details of production dynamics allows one to extract important information on the structure of the proton (parton densities) in regions of Q^2 and x otherwise unaccessible. Control of QCD at the current machines (the Tevatron at Fermilab) is therefore essential for the extrapolation of predictions to higher energies (say for applications at the future LHC, at CERN).

The key ingredients for the calculation of production rates and distributions in hadronic collisions are:

- the matrix elements for the hard, partonic process (e.g., $gg \to gg, gg \to b\bar{b}, q\bar{q}' \to W, \ldots$),
- the hadronic parton densities, discussed in the previous lecture

Then the production rate for a given final state H is given by a factorization formula similar to the one used to describe DIS:

$$d\sigma(p\bar{p} \to H + X) = \int dx_1\ dx_2 \sum_{i,j} f_i(x_1, Q)\ f_j(x_2.Q)\ d\hat{\sigma}(ij \to H) \quad (2.1)$$

where the parton densities f_i's are evaluated at a scale Q typical of the hard process under consideration. For example $Q \simeq M_{DY}$ for production of a Drell-Yan pair, $Q \simeq E_T$ for high transverse-energy (E_T) jets, $Q^2 \simeq p_T^2 + m_Q^2$ for high-p_T heavy quarks, etc.

In this lecture we will briefly explore three of the QCD phenomena currently studied in hadronic collisions: Drell-Yan, inclusive jets, and heavy quark production. More details can be found in ref. [1, 4].

2.1 Drell-Yan processes

While the Z boson has been recently studied with great precision by the LEP experiments, it was actually discovered, together with the W boson, by the CERN experiments UA1 and UA2 in $p\bar{p}$ collisions. W physics is now being studied in great detail at LEP2, but the best direct measurements of its mass by a single group still belong to $p\bar{p}$ experiments (CDF and D0 at the Tevatron). Even after the ultimate luminosity will have been accumulated at LEP2, with a great improvement in the determination of the parameters of the W boson, the monopoly of W studies will immediately return to hadron colliders, with the Tevatron data-taking resuming in the year 2000, and later on with the start of the LHC experiments.

Precision measurements of W production in hadronic collisions are important for several reasons:

- this is the only process in hadronic collisions which is known to NNLO accuracy
- the rapidity distribution of the charged leptons from W decays is sensitive to the ratio of the up and down quark densities, and can contribute to our understanding of the proton structure.
- deviations from the expected production rates of highly virtual W's ($p\bar{p} \to W^* \to e\nu$) are a possible signal of the existence of new W bosons, and therefore of new gauge interactions.

The partonic cross-section for the production of a W boson from the annihilation of a $q\bar{q}$ pair can be easily calculated, giving the following result [1, 4]:

$$\hat{\sigma}(q_i\bar{q}_j \to W) = \pi\ \frac{\sqrt{2}}{3}\ |V_{ij}|^2\ G_F\ M_W^2\ \delta(\hat{s} - M_W^2) = A_{ij}\ M_W^2\ \delta(\hat{s} - M_W^2) \quad (2.2)$$

where $\hat{s}$ is partonic center of mass energy squared, and V_{ij} is the element of the Cabibbo-Kobayashi-Maskawa matrix. The delta function comes from the $2 \to 1$ phase space, which forces the center-of-mass energy of the initial state to coincide with the W mass. It is useful to introduce the two

variables

$$\tau = \frac{\hat{s}}{S_{had}} \equiv x_1 x_2 \tag{2.3}$$

$$y = \frac{1}{2}\log\left(\frac{E_W + p_W^z}{E_W - p_W^z}\right) \equiv \frac{1}{2}\log\left(\frac{x_1}{x_2}\right) \tag{2.4}$$

where S_{had} is the hadronic center of mass energy squared. The variable y is called *rapidity*. For slowly moving objects it reduces to the standard velocity, but, contrary to the velocity, it transforms additively even at high energies under Lorentz boosts along the direction of motion. Written in terms of τ and y, the integration measure over the initial-state parton momenta becomes: $dx_1 dx_2 = d\tau dy$. Using this expression and eq. (2.2) in eq. (2.1), we obtain the following result for the LO total W production cross section:

$$\begin{aligned}\sigma_{DY} &= \sum_{i,j} \frac{\pi A_{ij}}{M_W^2}\,\tau \int_\tau^1 \frac{dx}{x}\; f_i(x)\; f_j\left(\frac{\tau}{x}\right) \\ &\equiv \sum_{i,j} \frac{\pi A_{ij}}{M_W^2}\tau \mathcal{L}_{ij}(\tau)\end{aligned} \tag{2.5}$$

where the function $\mathcal{L}_{ij}(\tau)$ is usually called *partonic luminosity*. In the case of $u\bar{d}$ collisions, the overall factor in front of this expression has a value of approximately 6.5 nb. It is interesting to study the partonic luminosity as a function of the hadronic CoM energy. This can be done by taking a simple approximation for the parton densities. Following the indications of the figures presented in the previous lecture, we shall assume that $f_i(x) \sim 1/x^{1+\delta}$, with $\delta < 1$. Then

$$\begin{aligned}\mathcal{L}(\tau) &= \int_\tau^1 \frac{dx}{x}\,\frac{1}{x^{1+\delta}}\left(\frac{x}{\tau}\right)^{1+\delta} = \frac{1}{\tau^{1+\delta}}\int_\tau^1 \frac{dx}{x} \\ &= \frac{1}{\tau^{1+\delta}}\;\log\left(\frac{1}{\tau}\right)\end{aligned} \tag{2.6}$$

and

$$\begin{aligned}\sigma_W &\sim \tau^{-\delta}\;\log\left(\frac{1}{\tau}\right) \\ &= \left(\frac{S_{had}}{M_W^2}\right)^{\delta}\;\log\left(\frac{S_{had}}{M_W^2}\right)\end{aligned} \tag{2.7}$$

The DY cross-section grows therefore at least logarithmically with the hadronic CM energy. This is to be compared with the behaviour of the Z production cross section in e^+e^- collisions, which is steeply diminuishing for values of s well above the production threshold. The reason for the different behaviour in hadronic collisions is that while the energy of the hadronic initial state grows, it will always be possible to find partons inside the hadrons with the appropriate energy to produce the W directly on-shell. The number of partons available for the production of a W is furthermore increasing with the increase in hadronic energy, since the larger the hadron energy, the smaller will be the value of hadron momentum fraction x necessary to produce the W. The increasing number of partons available at smaller and smaller values of x causes then the growth of the total W production cross section.

A comparison between the best available prediction for the production rates of W and Z bosons in hadronic collisions, and the experimental data, is shown in fig. 3. The experimental uncertainties will soon be dominated by the limited knowledge of the machine luminosity, and will exceed the accuracy of the NNLO predictions. This suggests that in the future the total rate of produced W bosons could be used as an accurate luminometer.

It is also interesting to note that an accurate measurement of the relative W and Z production rates (which is not affected by the knowledge of the total integrated luminosity, that will cancel in their ratio) provides a tool to measure the total W width. This can be seen from the following equation:

$$\Gamma_W = \frac{N^{obs}(Z \to e^+e^-)}{N^{obs}(W \to e^\pm\nu)}\left(\frac{\sigma_{W^\pm}}{\sigma_Z}\right)\left(\frac{\Gamma_{e\nu}^W}{\Gamma_{e^+e^-}^Z}\right)\Gamma_Z$$

measure — calculable — LEP/SLC

As of today, this technique provides the best measurement of Γ_W: $\Gamma_W = 2.06 \pm 0.06$ GeV, which is a factor of 5 more accurate than the current best direct measurements from LEP2.

2.2 W Rapidity Asymmetry

The measurement of the charge asymmetry in the rapidity distribution of W bosons produced in $p\bar{p}$

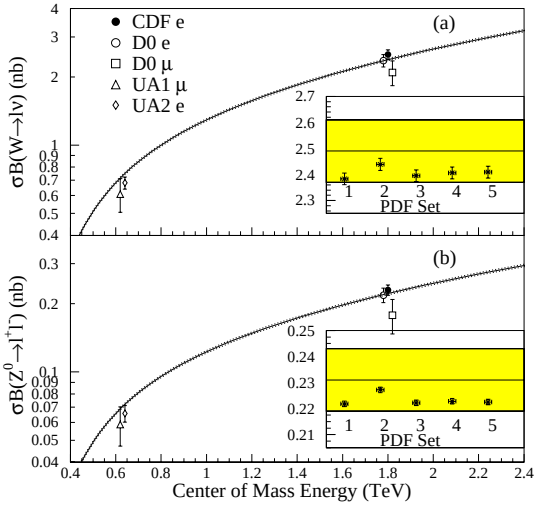

Figure 3: Comparison of measured (a) $\sigma \cdot B(W \to e\nu)$ and (b) $\sigma \cdot B(Z^0 \to e^+e^-)$ to 2-loop theoretical predictions using MRSA parton distribution functions. The UA1 and UA2 measurements and D0 measurements are offset horizontally by ± 0.02 TeV for clarity. In the inset, the shaded area shows the 1σ region of the CDF measurement; the stars show the predictions using various parton distribution function sets (1) MRSA, (2) MRSD0′, (3) MRSD-′, (4) MRSH and (5) CTEQ2M. The theoretical points include a common uncertainty in the predictions from choice of renormalization scale ($M_W/2$ to $2M_W$).

collisions can provide an important measurement of the ratio of the u-quark and d-quark momentum distributions. Using the formulas provided above, you can in fact easily check as an exercise that:

$$\frac{d\sigma_{W^+}}{dy} \propto f_u^p(x_1)\ f_{\bar{d}}^{\bar{p}}(x_2) + f_{\bar{d}}^p(x_1) f_u^{\bar{p}}(x_2) \quad (2.8)$$

$$\frac{d\sigma_{W^-}}{dy} \propto f_{\bar{u}}^p(x_1)\ f_d^{\bar{p}}(x_2) + f_d^p(x_1) f_{\bar{u}}^{\bar{p}}(x_2) \quad (2.9)$$

We can then construct the following charge asymmetry (assuming the dominance of the quark densities over the antiquark ones, which is valid in the kinematical region of interest for W production at the Tevatron):

$$A(y) = \frac{\frac{d\sigma_{W^+}}{dy} - \frac{d\sigma_{W^-}}{dy}}{\frac{d\sigma_{W^+}}{dy} + \frac{d\sigma_{W^-}}{dy}} = \frac{f_u^p(x_1)\ f_d^p(x_2) - f_d^p(x_1)\ f_u^p(x_2)}{f_u^p(x_1)\ f_d^p(x_2) + f_d^p(x_1)\ f_u^p(x_2)} \quad (2.10)$$

Setting $f_d(x) = f_u(x)\ R(x)$ we then get:

$$A(y) = \frac{R(x_2) - R(x_1)}{R(x_2) + R(x_1)}\ . \quad (2.11)$$

which measures the $R(x)$ ratio since $x_{1,2}$ are known in principle from the kinematics: $x_{1,2} = \sqrt{\tau}\exp(\pm y)$[2]. The current CDF data provide the most accurate measurement to date of this quantity (for more details, see ref. [4]).

2.3 Jet Production

Jet production is the hard process with the largest rate in hadronic collisions. For example, the cross section for producing at the Tevatron ($\sqrt{S_{had}} = 1.8$ TeV) jets of transverse energy $E_T^{jet} \lesssim 50$ GeV is of the order of a μb. This means 50 events/sec at the luminosities available at the Tevatron. The data collected at the Tevatron so far extend all the way up to the E_T values of the order of 450 GeV. These events are generated by collisions among partons which carry over 50% of the available $p\bar{p}$ energy, and allow to probe the shortest distances ever reached.

Data on jet production in hadronic collisions can be used for different purposes:

- They provide valuable test of QCD, since calculations are available up to the NLO [5].
- They allow to extract information on $f_{q,g}(x, Q^2)$ at large Q^2
- They allow to measure $\alpha_s(Q^2)$ over a huge range of Q^2
- They provide constraints on the point-like nature of quarks, and help setting limits on possible contact interactions, signalling the onset of new dynamical processes and the presence of new forces.
- 2-jet (or multi-jet) mass spectra can be used to search for production of new resonances,

[2] In practice one cannot determine $x_{1,2}$ with arbitrary precision on an event-by-event basis, since the longitudinal momentum of the neutrino cannot be easily measured. The actual measurement is therefore done by studying the charge asymmetry in the rapidity distribution of the charged lepton.

once again indicating the existence of new interactions beyond the SM.

The leading mechanisms for jet production in QCD are shown in fig. 4.

The 2-jet inclusive cross section can be obtained from the formula

$$d\sigma = \sum_{ijkl} dx_1\, dx_2\, f_i^{(H_1)}(x_1,\mu)\, f_j^{(H_2)}(x_2,\mu) \times \frac{d\hat{\sigma}_{ij\to k+l}}{d\Phi_2}\, d\Phi_2 \tag{2.12}$$

that has to be expressed in terms of the rapidity and transverse momentum of the quarks (or jets), in order to make contact with physical reality. The two-particle phase space is given by

$$d\Phi_2 = \frac{d^3k}{2k^0(2\pi)^3}\, 2\pi\, \delta((p_1+p_2-k)^2)\,, \tag{2.13}$$

and, in the CM of the colliding partons, we get

$$d\Phi_2 = \frac{1}{2(2\pi)^2}\, d^2k_T\, dy\; 2\,\delta(\hat{s}-4(k^0)^2\,)\,, \tag{2.14}$$

where k_T is the transverse momentum of the final-state partons. Here y is the rapidity of the produced parton in the parton CM frame. It is given by

$$y = \frac{y_1-y_2}{2} \tag{2.15}$$

where y_1 and y_2 are the rapidities of the produced partons in the laboratory frame (in fact, in any frame). One also introduces

$$y_0 = \frac{y_1+y_2}{2} = \frac{1}{2}\log\frac{x_1}{x_2}\,, \tag{2.16}$$

$$\tau = \frac{\hat{s}}{S_{had}} = x_1\, x_2\,. \tag{2.17}$$

With $dx_1\, dx_2 = dy_0\, d\tau$ we obtain:

$$d\sigma = \sum_{ijkl} dy_0\, \frac{1}{S_{had}}\, f_i^{(H_1)}(x_1,\mu)\, f_j^{(H_2)}(x_2,\mu) \times \frac{d\hat{\sigma}_{ij\to k+l}}{d\Phi_2}\, \frac{1}{2(2\pi)^2}\, 2\, dy\, d^2k_T \tag{2.18}$$

which can also be written as

$$\frac{d\sigma}{dy_1\, dy_2\, d^2k_T} = \frac{1}{S_{had}\; 2(2\pi)^2} \times \sum_{ijkl} f_i^{(H_1)}(x_1,\mu)\, f_j^{(H_2)}(x_2,\mu) \times \frac{d\hat{\sigma}_{ij\to k+l}}{d\Phi_2}\,. \tag{2.19}$$

The variables x_1, x_2 can be obtained from y_1, y_2 and k_T from the equations

$$y_0 = \frac{y_1+y_2}{2} \tag{2.20}$$

$$y = \frac{y_1-y_2}{2} \tag{2.21}$$

$$x_T = \frac{2k_T}{\sqrt{S_{had}}} \tag{2.22}$$

$$x_1 = x_T\, e^{y_0}\, \cosh y \tag{2.23}$$

$$x_2 = x_T\, e^{-y_0}\, \cosh y\,. \tag{2.24}$$

For the partonic variables, we need $\hat{s}$ and the scattering angle in the parton CM frame θ, since

$$t = -\frac{\hat{s}}{2}\,(1-\cos\theta)\,, \qquad u = -\frac{\hat{s}}{2}\,(1+\cos\theta)\,. \tag{2.25}$$

Neglecting the parton masses, you can show that the rapidity can also be written as:

$$y = -\log\tan\frac{\theta}{2} \equiv \eta\,, \tag{2.26}$$

with η being usually referred to as pseudorapidity.

The leading-order Born cross sections for parton parton scattering are reported in table 1.

Process	$\frac{d\hat{\sigma}}{d\hat{\Phi}_2}$
$qq' \to qq'$	$\frac{1}{2\hat{s}}\frac{4}{9}\frac{\hat{s}^2+\hat{u}^2}{\hat{t}^2}$
$qq \to qq$	$\frac{1}{2}\frac{1}{2\hat{s}}\left[\frac{4}{9}\left(\frac{\hat{s}^2+\hat{u}^2}{\hat{t}^2}+\frac{\hat{s}^2+\hat{t}^2}{\hat{u}^2}\right)-\frac{8}{27}\frac{\hat{s}^2}{\hat{u}\hat{t}}\right]$
$q\bar{q} \to q'\bar{q}'$	$\frac{1}{2\hat{s}}\frac{4}{9}\frac{\hat{t}^2+\hat{u}^2}{\hat{s}^2}$
$q\bar{q} \to q\bar{q}$	$\frac{1}{2\hat{s}}\left[\frac{4}{9}\left(\frac{\hat{s}^2+\hat{u}^2}{\hat{t}^2}+\frac{\hat{t}^2+\hat{u}^2}{\hat{s}^2}\right)-\frac{8}{27}\frac{\hat{u}^2}{\hat{s}\hat{t}}\right]$
$q\bar{q} \to gg$	$\frac{1}{2}\frac{1}{2\hat{s}}\left[\frac{32}{27}\frac{\hat{t}^2+\hat{u}^2}{\hat{t}\hat{u}}-\frac{8}{3}\frac{\hat{t}^2+\hat{u}^2}{\hat{s}^2}\right]$
$gg \to q\bar{q}$	$\frac{1}{2\hat{s}}\left[\frac{1}{6}\frac{\hat{t}^2+\hat{u}^2}{\hat{t}\hat{u}}-\frac{3}{8}\frac{\hat{t}^2+\hat{u}^2}{\hat{s}^2}\right]$
$gq \to gq$	$\frac{1}{2\hat{s}}\left[-\frac{4}{9}\frac{\hat{s}^2+\hat{u}^2}{\hat{s}\hat{u}}+\frac{\hat{u}^2+\hat{s}^2}{\hat{t}^2}\right]$
$gg \to gg$	$\frac{1}{2}\frac{1}{2\hat{s}}\frac{9}{2}\left(3-\frac{\hat{t}\hat{u}}{\hat{s}^2}-\frac{\hat{s}\hat{u}}{\hat{t}^2}-\frac{\hat{s}\hat{t}}{\hat{u}^2}\right)$

Table 1: Cross sections for light parton scattering. The notation is $p_1\, p_2 \to k\, l$, $\hat{s} = (p_1+p_2)^2$, $\hat{t} = (p_1-k)^2$, $\hat{u} = (p_1-l)^2$.

It is interesting to note that a good approximation to the exact results can be easily obtained by applying a simplified set of Feynman rules valid in the limit of soft-gluon emission. In this limit,

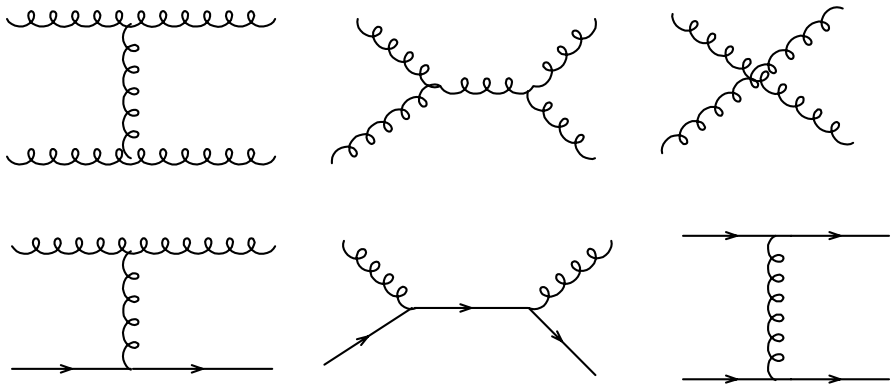

Figure 4: Representative diagrams for the production of jet pairs in hadronic collisions.

the vertex for emission of a gluon from a quark line is given by:

$$g\ \lambda^a_{ij}\ 2p^\mu \tag{2.27}$$

This is easy to prove, realising that the interaction vertex, aside from the obvious colour factor, is just given by the current:

$$\bar{u}(p')\gamma_\mu u(p) \tag{2.28}$$

where p and p' are the quark momenta before and after the gluon emission. In the case of soft-gluon emission, the quark momentum is left to first approximation unaltered. Setting $p' = p$, one just obtains the expression $\bar{u}(p)\gamma_\mu u(p)$, which is equal to $2p_\mu$ from the standard normalization of massless spinors. It is easy to prove that a similar expression holds in the case of soft-gluon emission from a hard gluon:

$$igf^{abc}\ 2p^\mu\ g^{\nu\rho} \tag{2.29}$$

where the quark colour factor was replaced by the gluon one, μ is the Lorentz index of the emitted gluon, and ν, ρ are the Lorentz indices of the hard gluon before and after the emission.

Based on the fact that even at 90° $min(|t|, |u|)$ does not exceed $s/2$, and that therefore everything else being equal a propagator in the t or u channel contributes to the square of an amplitude 4 times more than a propagator in the s channel, it is reasonable to assume that the amplitudes are dominated by the diagrams with a gluon exchanged in the t (or u) channel. It is easy to calculate the amplitudes in this limit using the soft-gluon approximation.

For example, the amplitude for the exchange of a soft gluon among a qq' pair is given by:

$$\begin{aligned}(\lambda^a_{ij})\ (\lambda^a_{kl})\, 2p_\mu\ \frac{1}{t}\ 2p'_\mu &= \lambda^a_{ij}\ \lambda^a_{kl}\ \frac{4p\cdot p'}{t} \\ &= \frac{2s}{t}\ \lambda^a_{ij}\ \lambda^a_{kl}\end{aligned} \tag{2.30}$$

The p_μ and p'_μ factors represent the coupling of the exchanged gluon to the q and q' quark lines, respectively (see eq. (2.27). Squaring, and summing and averaging over spins and colours, gives

$$\overline{\sum_{\text{colours,spin}}} |M_{qq'}|^2 \ =\ \frac{1}{N^2}\ \left(\frac{N^2-1}{4}\right)\ \frac{4s^2}{t^2} = \frac{8}{9}\,\frac{s^2}{t^2} \tag{2.31}$$

Since for this process the diagram with a t-channel gluon exchange is symmetric for $s \leftrightarrow u$ exchange, and since $u \to -s$ in the $t \to 0$ limit, the above result can be rewritten in an explicitly (s, u) symmetric way as

$$\frac{4}{9}\,\frac{s^2+u^2}{t^2} \tag{2.32}$$

which indeed exactly agrees with the result of the exact calculation, as given in table 1. The corrections which appear from s or u gluon exchange when the quark flavours are the same or when we study a $q\bar{q}$ process are small, as can be seen by comparing the above result to the expressions in the table.

As another example we consider the case of $qg \to qg$ scattering. The amplitude will be exactly the same as in the $qq' \to qq'$ case, up to the different colour factors. A simple calculation

then gives:

$$\overline{\sum_{\text{colours,spin}}} |M_{qg}|^2 \;=\; \frac{9}{4}\,\overline{\sum}|M_{qq'}|^2 = \frac{s^2+u^2}{t^2} \tag{2.33}$$

The exact result is

$$\frac{u^2+s^2}{t^2} - \frac{4}{9}\,\frac{u^2+s^2}{us} \tag{2.34}$$

which even at 90°, the point where the t-channel exchange approximation is worse, only differs from this latter by no more than 25%.

As a final example we consider the case of $gg \to gg$ scattering, which in our approximation gives:

$$\overline{\sum}|M_{gg}|^2 = \frac{9}{2}\,\frac{s^2}{t^2} \tag{2.35}$$

By $u \leftrightarrow t$ symmetry we should expect the simple improvement:

$$\overline{\sum}|M_{gg}|^2 \sim \frac{9}{2}\,\left(\frac{s^2}{t^2}+\frac{s^2}{u^2}\right). \tag{2.36}$$

This only differs by 20% from the exact result at 90°.

Notice that at small t the following relation holds:

$$\hat\sigma_{gg} : \hat\sigma_{qg} : \hat\sigma_{q\bar q} = \left(\frac{9}{4}\right) : 1 : \left(\frac{4}{9}\right) \tag{2.37}$$

The 9/4 factors are simply the ratios of the colour factors for the coupling to gluons of a gluon (C_A) and of a quark (T_F), after including the respective colour-average factors ($1/(N^2-1)$ for the gluon, and $1/N$ for the quark). Using eq. (2.37), we can then write:

$$\begin{aligned} d\sigma_{hadr} &= \int dx_1\; dx_2 \sum_{i,j}\; f_i(x_1)\; f_j(x_2)\; d\hat\sigma_{ij} \\ &= \int dx_1\; dx_2\, F(x_1)\; F(x_2)\; d\hat\sigma_{gg}(gg\to \text{jets}) \end{aligned} \tag{2.38}$$

where the object:

$$F(x) = f_g(x) + \frac{4}{9}\sum_f\; [q_f(x)+\bar q_f(x)] \tag{2.39}$$

is usually called the *effective structure function*. This result indicates that the measurement of the inclusive jet cross section does not allow in principle to disentangle the independent contribution of the various partonic components of the proton, unless of course one is considering a kinematical region where the production is dominated by a single process. The relative contributions of the different channels, as predicted using the global fits of parton densities available in the literature, are shown in fig. 5

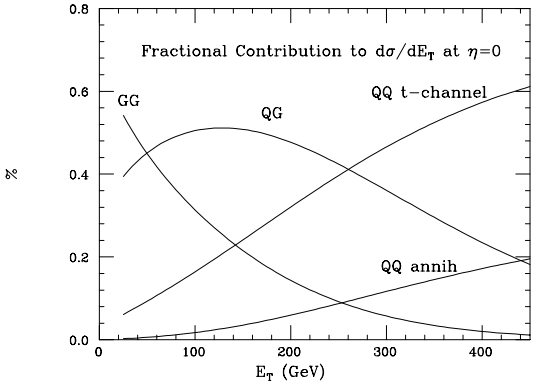

Figure 5: Relative contribution to the inclusive jet-E_T rates from the different production channels.

2.3.1 Comparison of QCD with Tevatron jet data

At the Tevatron, jets up to 450 GeV transverse momentum have been observed [6, 7]. That is $x \gtrsim 0.5$ and $Q^2 \simeq 160{,}000$ GeV^2. This is a domain of x and Q^2 not accessible to DIS experiments, such as those running at HERA. The current agreement between theory and data is at the level of 30 % over 8 orders of magnitude of cross-section, from $E_T \sim 20$ to $E_T \sim 450$ GeV (see fig. 6) In spite of the general good agreement, a large dependence on the chosen set of parton densities is present, as shown in fig. 7. The presence of this uncertainty limits the use of high-E_T jet data to set constraints on possible new physics.

An important question is therefore the following: to which extent do independent measurements of parton densities constrain the knowledge of PDFs at large-x, and what is the residual uncertainty on the jet E_T distributions? To address this issue, let us first show what is the relative contribution of different initial state par-

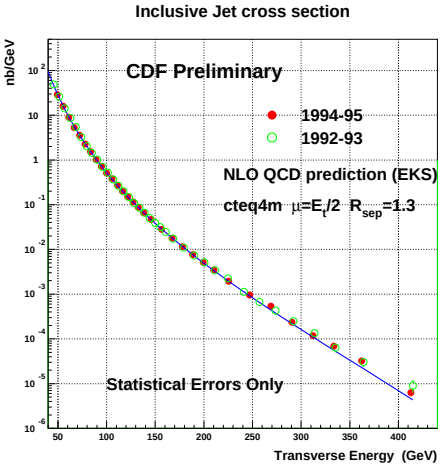

Figure 6: Inclusive jet transverse energy (E_T) distribution as measured by CDF, compared to the absolute NLO QCD calculation.

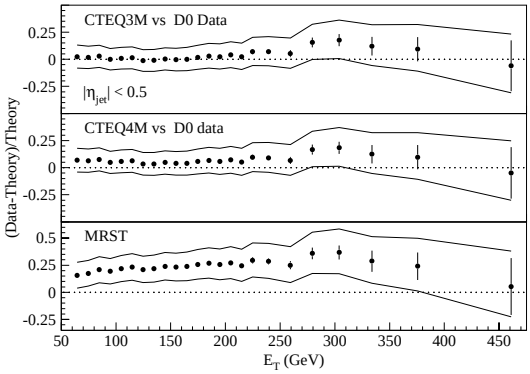

Figure 7: Deviations of QCD predictions from D0 jet data for various sets of PDFs.

tons to the jet cross section. This was plotted in fig. 5, where some standard PDF set (CTEQ4M in this case) was chosen. At the largest energies accessible to today's Tevatron data, 80% of the jets are produced by collisions involving only initial state quarks. The remaining 20% comes from processes where at least one gluon was present in the initial state.

Quark densities at large-x quarks are constrained by DIS data to within few percent, leading to an overall uncertainty on the high-E_T jet rate of at most 5%. What is uncertainty on the remaining 20% coming from gluon-induced processes? How are we guaranteed that the gluons

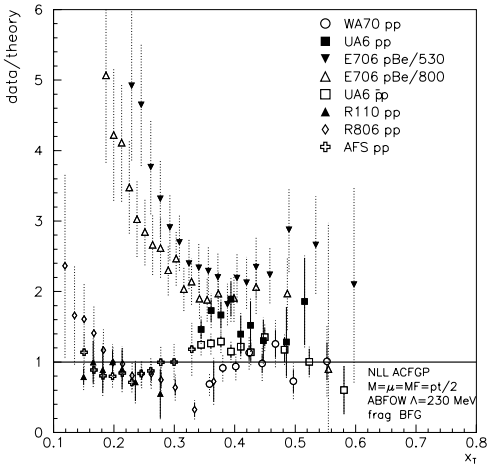

Figure 8: Relative deviations between NLO QCD and prompt photon data, as a function of $x_T = 2p_T/\sqrt{S}$, for various fixed target experiments.

are known to better than a factor of 2, limiting the overall uncertainty to 20-30%?

The only independent constraint on $f_g(x, Q^2)$ comes from fixed-target production of prompt photons. This process is induced at LO by two mechanisms:

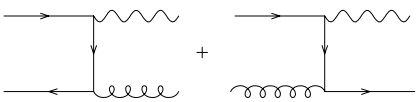

In pN collisions $g(x) \gg \bar{q}(x)$, and

$$\frac{d\sigma}{dE_T}(qg \to q\gamma) \gg \frac{d\sigma}{dE_T}(q\bar{q} \to g\gamma) \qquad (2.40)$$

Data from FNAL and CERN fixed target experiments are used to extract $f_g(x, Q^2)$ at large x.

- How reliable are these extractions?
- How reliable is the theory of prompt-γ production?

Unfortunately, a comparison of data and NLO theory shows inconsistencies at small E_T between the various experiments, as shown in fig. 8 [8]

As a possible explanation for these discrepancies, the presence of a large non-perturbative

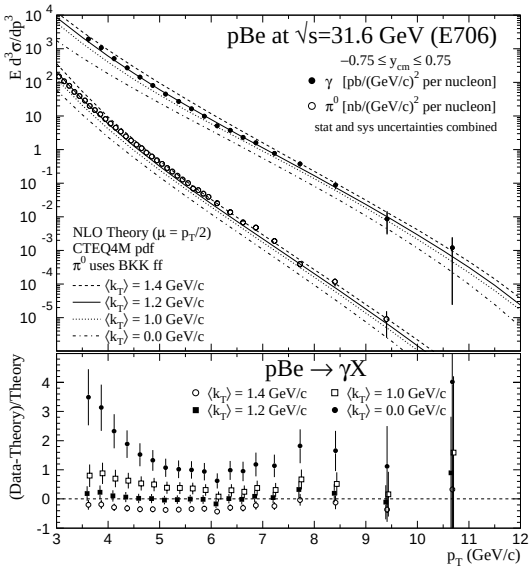

Figure 9: Comparison of E706 data [9] with NLO QCD, before and after inclusion of an intrinsic-k_T.

contribution from the intrinsic k_T of partons inside the nucleon has been suggested [10]. The effect of this intrinsic k_T is to smear the p_T distribution, as shown in fig. 9. Inclusion of these effects, however, has a big impact also on the rate at large E_T (i.e. $x \sim 0.6$). Due to the large size of the effects, and to their intrinsic non-perturbative nature (which means that they cannot be understood from first principles, and need to be described by ad hoc models), it is hard to trust the theoretical predictions obtained in this way, and to claim that prompt photons provide a reliable way of extracting the gluon content of the proton at large x. Recent theoretical improvements, such as the resummation of large-x_T logarithms [11, 12, 13], should help understanding the large-x problem, but more work is necessary. In conclusion, the issue of the large-x behaviour of $f_g(x)$ is still an open problem.

Concerning the possible eccess observed by CDF in its highest E_T jet data, additional input will be available with the the data from the upcoming run of the Tevatron (due to start in the Summer 2000), thanks to an increased energy ($\sqrt{S} \to 2$ TeV, 10% increase). Should the eccess be due to a problem with the gluon density at large x, a discrepancy similar to the one observed at 1.8 TeV will appear at jet E_T values 10% larger. If the eccess is instead due to really new phenomena, one expects the excess to appear at the same value of E_T as seen in the data at 1.8 TeV. Time will tell!

2.3.2 630/1800 GeV cross-section ratios

The Tevatron has been able to run also at a reduced CM energy of 630 GeV. Data collected at this energy provide another interesting jet observable, namely the ratio of cross-sections at 630 and 1800 GeV, plotted as a function of the rescaled variable x_T:

$$R(x_T = \frac{2E_T}{\sqrt{S}}) \;=\; \frac{[E_T^3\; ds/dE_T]_{\sqrt{S}=630}}{[E_T^3\; ds/dE_T]_{\sqrt{S}=1800}} \quad (2.41)$$

It is expected that a large fraction of theoretical and experimental systematics will cancel in this ratio. In the exact scaling limit, $R(x_T) = 1$. Deviations from 1 arise from scaling violations in α_s and in the parton densities. The NLO theoretical uncertainity on this ratio is better than 10%.

CDF and D0 observe instead serious deviations from theory at $x_T \lesssim 0.15$ ($E_T^{630} \lesssim 50$ GeV), as shown in fig. 10 and 11. What's more, the pattern of deviations is inconsistent between the two experiments. (For previous studies of power-suppressed effects in the jet cross-sections and ratios, see e.g. [14])

It is easy to get a good approximation for the expected ratio of cross-sections. Let us approximate the inclusive jet cross-section with the value of the differential cross-section at $y = 0$ for both jets. In this case, at LO, one gets:

$$R(x_T) \;=\; \frac{\Sigma(x_T,\; 630\text{ GeV})}{\Sigma(x_T,\; 1800\text{ GeV})} \quad (2.42)$$

with

$$\Sigma(x_T, \sqrt{S}) \;=\; \alpha_s^2(\mu)\; F^2(x_T, \mu), \quad (2.43)$$

for $\mu \sim x_T\sqrt{S}/2$ and

$$F(x) = G(x) + \frac{4}{9}\sum_{q,\bar{q}}\; \left[Q(x) + \bar{Q}(x)\right] \quad (2.44)$$

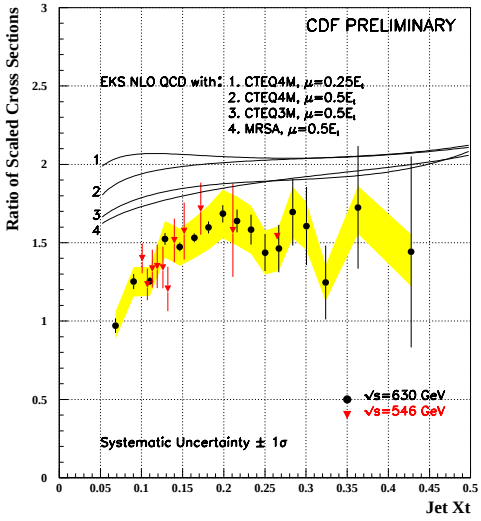

Figure 10: 630 to 1800 GeV x_T distribution ratios at CDF, compared to NLO QCD

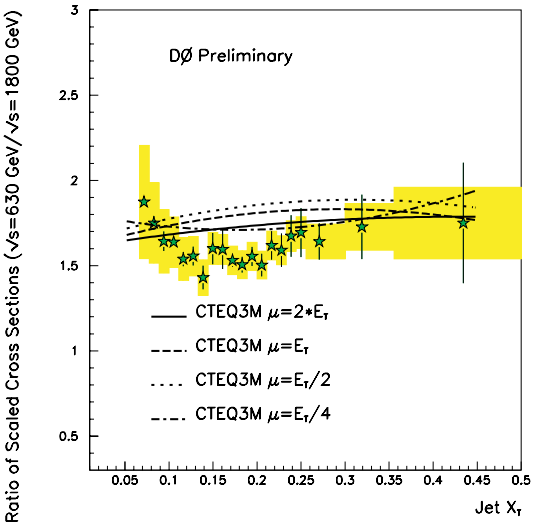

Figure 11: 630 to 1800 GeV x_T distribution ratios at D0, compared to NLO QCD

It turns out that this is indeed a very good approximation to the exact result, and in any case Σ does embody most of the scaling violations expected of the exact cross-section.

Any change in the jet energy, due to either detector effects or to unaccounted-for theoretical effects, would lead to a correction to Σ of the following form:

$$\Sigma(x_T, \sqrt{S}) \to \Sigma(x_T, \sqrt{S}) \times \left(1 + \frac{A}{E_T}\right) , \tag{2.45}$$

Possible sources of $A \neq 0$ include:

- Energy lost outside the jet cone ($A < 0$)
- Energy from the underlying event inside the jet cone ($A > 0$)
- Intrinsic k_T effects ($A > 0$)

PT contributions to the energy gain/loss can be evaluated and removed. However this can be done at LO only, since they are effects of $\mathcal{O}(\alpha_s^3)$ in PT. Some energy changes induced by non-PT effects can be extracted from data and corrected for. E.g. the energy deposited in the cone by at least a part of the Minimum Bias underlying event. Finally, there is class of non-PT effects (e.g. parton recombinations with the beam fragments and with nearby jets) which are out of control.

When the experiments correct for these effects before the comparison with the data, they may be left with a residual A of arbitrary sign, depending on whether the correction is over- or under-done. This seems like a plausible explanation for why CDF and D0 get a discrepancy of opposite sign relative to the data.

Is the scale of the discrepancy reasonable? The scale for all these effects is $\Lambda \sim \mathcal{O}(1\text{ GeV})$. Assuming a $1/E_T^n$ fall-off of the cross-section, ones gets $A \sim n\Lambda$. Values of $A \sim 5$ GeV should therefore NOT be surprising.

For $A \sim \pm 5$ GeV the effects are large, as shown in Fig. 12, and can be consistent with the deviations observed by CDF and D0.

Fig. 13 shows a fit of the CDF data performed using the exact NLO jet cross-section (CTEQ3M, $\mu = E_T/2$), parameterised by an additional constant shift in the jet energy. A good fit is obtained with a shift in the parton-level jet energy of -2.8 GeV, which is a plausible value given the current uncertainties on the higher-

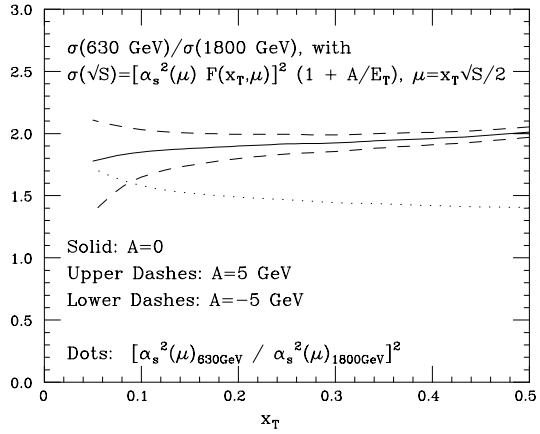

Figure 12: 630 to 1800 GeV x_T distribution ratios at D0, compared to NLO QCD

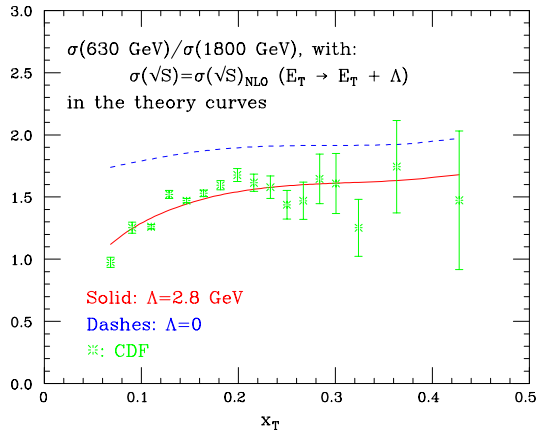

Figure 13: Fit of the jet-energy shifted NLO QCD calculation for the 630 to 1800 GeV x_T distribution ratios at CDF

order corrections to the jet development and the underlying event structure.

Conclusions on the jet data at the Tevatron:

- There is no evidence for departures from QCD
- Current discrepancies (E_T spectrum at CDF, x_T ratios 630/1800 at both CDF and D0) are within theoretical and experimental uncertainties once proper account is taken of:
  - true uncertainties on the extraction of the gluon density
  - power corrections

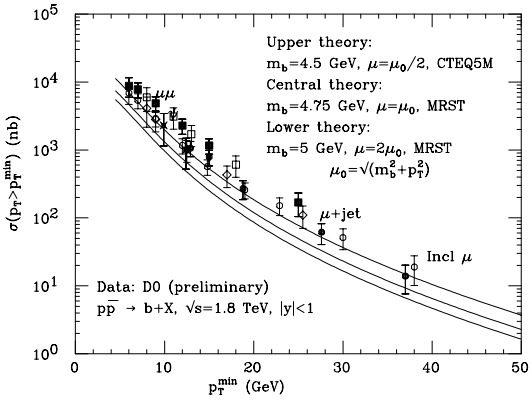

Figure 14: Comparison of NLO QCD with D0 data for the integrated b-quark p_T spectrum.

2.4 Bottom quark production at the Tevatron

The prediction of bottom cross-sections in hadronic collisions is a sore point for perturbative QCD. NLO calculations have been available for several years now for the total cross sections [15], for single-inclusive distributions [16] and for correlations [17]. As pointed out in the original papers [15], the inclusion of NLO corrections increases the rates by factors of order 2, and leaves a large scale dependence (of order 2 or more, if renormalisation and factorisation scales are varied independently). As a result, any comparison with data (for a recent complete review, see ref. [18]) will at best be qualitative, and certainly will not provide a compelling test of the theory. The current comparison of single-inclusive rates, as measured by CDF and D0, with NLO QCD, is summarised in Fig. 14 (D0 [19]) and Fig. 15 (CDF).

Within the theoretical uncertainties, the agreement with data is acceptable. The comparison indicates that smaller values of the renormalisation and factorization scales are favoured. Indeed, if one were to push the scale down to values of the order of $\sqrt{m_b^2 + p_T^2}/4$, the theory curve would exactly overlap the data. In spite of the large uncertainty in the prediction of the absolute rates, the NLO predictions for the shapes

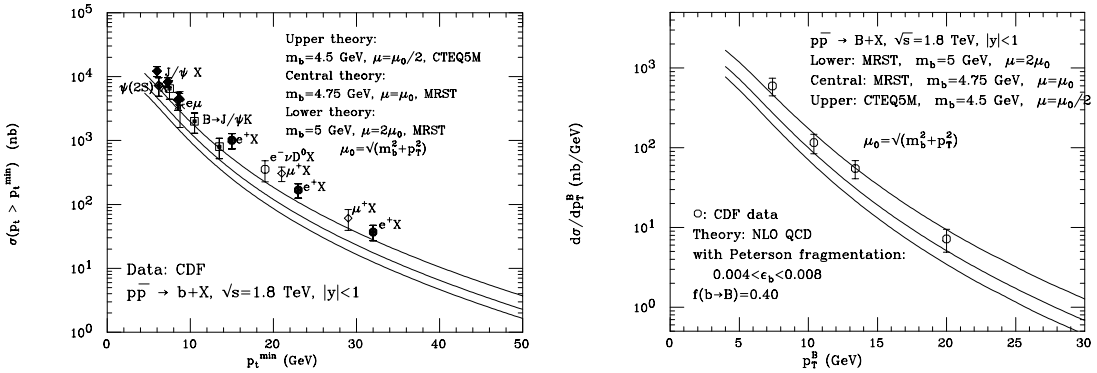

Figure 15: Comparison of NLO QCD with CDF data for the integrated b-quark p_T spectrum (left) and for the differential B-meson p_T distribution (right).

of the $b\bar{b}$ correlations are better defined. Evidence was given in the past [18], and confirmed recently in [19], that NLO QCD provides a good description of the shape of azimuthal $b\bar{b}$ correlations. It was shown by CDF that the theory provides also a good description of the $b\bar{b}$ rapidity correlations [20]. All of these observations make therefore rather intriguing the anomaly observed by D0 in the inclusive forward production of b quarks [21]. In this paper, D0 reports a factor of 2 excess in the production of forward b's, relative to what expected by extrapolating the rate measured in the central rapidity region. Possible mechanisms have been proposed to increase the expected rates for forward production of B mesons (e.g. a harder non-perturbative fragmentation function [22]), but none of them can explain the large effect observed by D0.

Recent progress in theory [23, 24] has led to the the resummation of the large-p_T logarithms appearing at all orders in PT ($[\alpha_s \log(p_T/m_b)]^n$). The main result of these additional contributions is the improvement in the scale dependence of the results, compared to the fixed-order NLO calculation. In addition, in the region of p_T where the data are available, the resummed calculation predicts a rate which is closer to the upper estimate of the NLO result, obtained with the choice of the *low* scale $\mu = \mu_0/2$. This is shown in fig. 16. The result goes in the right direction to agree with the CDF and D0 data.

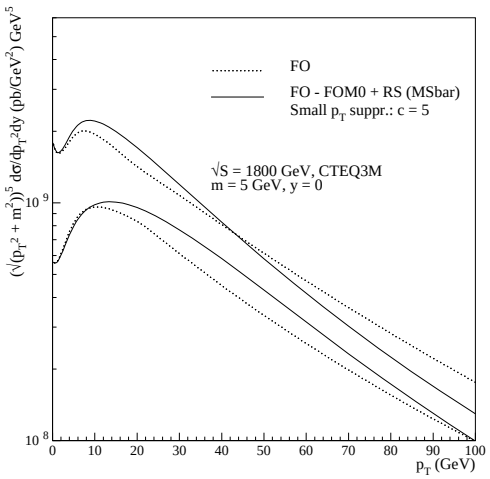

Figure 16: The differential p_T spectrum for bottom quarks at the Tevatron, as predicted by NLO QCD (dotted lines), and by the NLL resummed calculation of Cacciari et al [24] (solid lines). The bands represent the range in the predictions induced by the variation of the renormalization and factorization scales in the interval $\mu_0/2 < \mu < 2\mu_0$, with $\mu_0^2 = p_T^2 + m^2$.

2.5 Top quark production at the Tevatron

Theoretical predictions for $t\bar{t}$ production at the Tevatron are expected to be rather robust, given the large value of the top mass and the correspondingly small value of the coupling, $\alpha_s(m_{top})$, appearing in the QCD perturbative expansion. The next-to-leading-log (NLL) resummation of Sudakov threshold effects has been carried out in

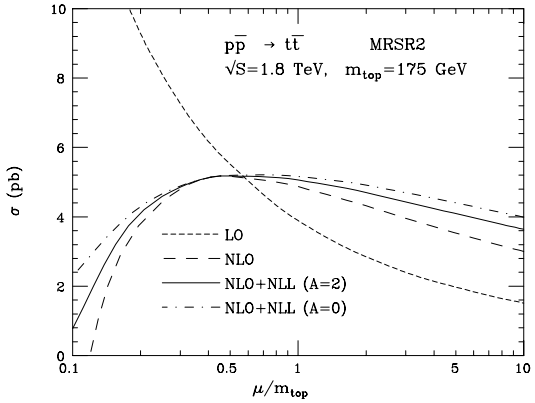

Figure 17: Scale dependence of $\sigma_{t\bar{t}}$ at the Tevatron (1.8 TeV), for various degrees of accuracy in the QCD calculation.

the past year [11, 25] Results indicate a good reduction in scale uncertainty, to the level of $\pm 5\%$, as shown in Fig. 17 [25]

In addition to the scale-variation uncertainty, a $\pm 7\%$ variation in the theoretical predictions is present due to the choice of PDF's (MRST: [26]; CTEQ5: [27]). The NLO+NLL results from [25], using the prescription for the inverse Mellin transform introduced in [28], are given in the following table:

PDF	$\mu = m_{top}/2$	$\mu = m_{top}$	$\mu = 2m_{top}$
MRST	5.04	4.92	4.57
MRST$g\uparrow$	5.22	5.09	4.72
MRST$g\downarrow$	4.90	4.79	4.45
MRST$\alpha_s\downarrow$	4.84	4.74	4.42
MRST$\alpha_s\uparrow$	5.20	5.07	4.68
CTEQ5M	5.41	5.30	4.91
CTEQ5HJ	5.61	5.50	5.10

A new determination of the $t\bar{t}$ cross-section was recently presented by CDF. The new value is approximately 1 standard deviation lower than the previous one [29], and in much better agreement with the QCD predictions. The overall cross-section averages from CDF and D0 (in this last case rescaled to $m_{top} = 175$ GeV) are shown in Table 2, and compared to various theoretical results appeared in the literature. Now that the CDF number has come down a bit, the average of the experimental determinations (5.9 ± 1.3 pb) is within less than one standard deviation from the QCD NLO+NLL resummed result of 5.0 ± 0.6 pb, extracted from the previous reslts, with scale and PDF uncertainties added linearly. It is interesting to notice that both CDF [29] and D0 [31] report significantly lower values for $\sigma(t\bar{t})$ in the single-lepton plus jets channels than in the all-jet or dilepton ones. These lower values are in closer agreement with QCD than the overall average. It is clearly premature to draw any conclusion on this small discrepancy between the determinations obtained using the various channels. Several studies of kinematical properties of top final states have been presented by CDF and D0. All results are in good agreement with the predictions from NLO QCD [34].

Acknowledgements

It is a pleasure to thank the organizers of this School, for the generous hospitality and for the the successful efforts made to provide a great environment for physics discussions and for a pleasant time as well.

References

[1] V. Barger and R.J.N. Phillips, Collider Physics, Addison Wesley (1987).

[2] R. Field, Applications of Perturbative QCD, Addison Wesley (1989).

[3] Yu.L. Dokshitzer, V.A. Khoze, A.H. Mueller and S.I. Troyan, Basics of Perturbative QCD, Editions Frontieres (1991).

[4] R.K. Ellis, W.J. Stirling and B.R. Webber: QCD and Collider Physics, Cambridge University Press (1996).

[5] F. Aversa, P. Chiappetta, M. Greco and J.Ph. Guillet, Nucl. Phys. **327** (1989) 105;
S.D. Ellis, Z. Kunszt and D.E. Soper, Phys. Rev. Lett. **64**, 2121 (1990);
W.T. Giele, E.W. Glover and D.A. Kosower, Nucl. Phys. **B403**, 633 (1993) hep-ph/9302225.

[6] F. Abe et al., CDF Collaboration, Phys. Rev. Lett. **77** (1996) 438.

[7] B. Abbott et al., DØ Collaboration, `hep-ex/9807018.`

[8] P. Aurenche, et al., `hep-ph/9811382`

CDF	D0	BCMN	BC	K
6.5 ± 1.5	5.4 ± 1.5	5.0 ± 0.6	$5.57^{+0.07}_{-0.42}$	7

Table 2: $t\bar{t}$ cross-sections, in pb, for $m_{top} = 175$ GeV. CDF: [30]; D0: [31]; BCMN: [28]; BC: [32]; K: [33]

[9] L. Apanasevich et al., E706 Collaboration, Phys. Rev. Lett. **81** (1998) 2642.

[10] L. Apanasevich et al., Phys. Rev. **59** (1999) 074007.

[11] N. Kidonakis and G. Sterman, Nucl. Phys. **B505**, 321 (1997) hep-ph/9705234.

[12] E. Laenen, G. Oderda and G. Sterman, Phys. Lett. **B438**, 173 (1998) hep-ph/9806467.

[13] S. Catani, M.L. Mangano and P. Nason, JHEP **07**, 024 (1998) hep-ph/9806484;
S. Catani, M.L. Mangano, P. Nason, C. Oleari and W. Vogelsang, JHEP **03**, 025 (1999) hep-ph/9903436.

[14] D. Soper, `hep-ph/9706320`, and D. Soper, J. Huston, work in progress.

[15] P. Nason, S. Dawson and R. K. Ellis, Nucl. Phys. **B303** (1988) 607;
W. Beenakker, H. Kuijf, W.L. van Neerven and J. Smith, Phys. Rev. **D40** (1989) 54.

[16] P. Nason, S. Dawson and R. K. Ellis, Nucl. Phys. **B327** (1989) 49, erratum *ibid.* **B335** (1990) 260;
W. Beenakker, W. L. van Neerven, R. Meng, G. A. Schuler and J. Smith, Nucl. Phys. **B351** (1991) 507.

[17] M.L. Mangano, P. Nason and G. Ridolfi, Nucl. Phys. **B373** (1992) 295.

[18] S. Frixione, M.L. Mangano, P. Nason and G. Ridolfi, hep-ph/9702287;
S. Frixione, M.L. Mangano, P. Nason and G. Ridolfi, Nucl. Phys. **B431**, 453 (1994).

[19] B. Abbott *et al.* [D0 Collaboration], hep-ex/9905024.

[20] F. Abe *et al.* [CDF Collaboration], FERMILAB-PUB-98-392-E, to appear on Phys. Rev. D.

[21] B. Abbott *et al.* [D0 Collaboration], hep-ex/9907029.

[22] M.L. Mangano, hep-ph/9711337.

[23] F.I. Olness, R.J. Scalise and W. Tung, Phys. Rev. **D59**, 014506 (1999) hep-ph/9712494.

[24] M. Cacciari, M. Greco and P. Nason, JHEP **05**, 007 (1998) hep-ph/9803400.

[25] R. Bonciani, S. Catani, M.L. Mangano and P. Nason, Nucl. Phys. **B529**, 424 (1998) hep-ph/9801375.

[26] A.D. Martin, R.G. Roberts, W.J. Stirling and R.S. Thorne, Eur. Phys. J. **C4**, 463 (1998) hep-ph/9803445.

[27] H.L. Lai *et al.* [CTEQ Collaboration], hep-ph/9903282.

[28] S. Catani, M.L. Mangano, P. Nason and L. Trentadue, Nucl. Phys. **B478**, 273 (1996) hep-ph/9604351;
S. Catani, M.L. Mangano, P. Nason and L. Trentadue, Phys. Lett. **B378**, 329 (1996) hep-ph/9602208.

[29] F. Abe *et al.* [CDF Collaboration], Phys. Rev. Lett. **80**, 2779 (1998) hep-ex/9802017.

[30] F. Ptohos, for the CDF Collab., presented at the 1999 EPS COnference on HEP, Tampere July 15-21 1999.

[31] B. Abbott *et al.* [D0 Collaboration], Phys. Rev. **D60**, 012001 (1999) hep-ex/9808034.

[32] E.L. Berger and H. Contopanagos, Phys. Rev. **D57**, 253 (1998) hep-ph/9706206.

[33] N. Kidonakis, hep-ph/9904507.

[34] S. Frixione, M.L. Mangano, P. Nason and G. Ridolfi, Phys. Lett. **B351**, 555 (1995) hep-ph/9503213.